NEW ARTIFICIAL TANGENTIAL MOTIONS FOR PARAMETRIC FINITE ELEMENT APPROXIMATION OF SURFACE EVOLUTION

BEIPING DUAN* AND BUYANG LI†

Abstract. A new class of parametric finite element methods, with a new type of artificial tangential velocity constructed at the continuous level, is proposed for solving surface evolution under geometric flows. The method is constructed by coupling the normal velocity of the geometric flow with an artificial tangential velocity determined by a harmonic map from a fixed reference surface $\mathcal{M}$ to the unknown surface $\Gamma(t)$, formulated at the continuous level as a system of geometric partial differential equations in terms of a Lagrange multiplier. Since the harmonic map is almost angle-preserving, the new method could preserve the mesh quality, i.e., the shapes of the triangles, as long as the mesh quality of the reference surface is good. Extensive numerical experiments and benchmark examples are presented to demonstrate the convergence of the proposed method and the advantages of the method in preserving the mesh quality of the surfaces for mean curvature flow and surface diffusion, in comparison with other available methods such as the parametric finite element methods proposed by Barrett, Garcke & Nürnberg in 2008, and the DeTurck flow techniques proposed by Elliott & Fritz in 2017.

Key words. Surface evolution, geometric flow, mean curvature flow, surface diffusion, parametric finite element method, artificial tangential velocity

AMS subject classifications. 53E10, 53E40, 65M60, 35K55

1. Introduction.

Surface evolution under geometric flows, including mean curvature flow, surface diffusion, elastic flow (also called Willmore flow), etc., frequently appear in mathematics and natural sciences. The evolution of an d-dimensional smooth hypersurface $\Gamma(t)$ in $\mathbb{R}^{d+1}$ under geometric flows can be described by the geometric evolution equation

$$\frac{\partial X(p,t)}{\partial t} = v(X(p,t),t), \quad \forall\, p \in \mathcal{M}, \tag{1.1}$$

where $X(p,t) : \mathcal{M} \to \mathbb{R}^{d+1}$ denotes the parametrization of surface from a reference surface $\mathcal{M}$, which describes the surface

$$\Gamma(t) = \{X(p,t) : p \in \mathcal{M}\}$$

as well as the trajectory $\{X(p,t) : t \in [0,T]\}$ of a particle $p \in \mathcal{M}$, and $v(\cdot,t)$ denotes a $(d+1)$-dimensional vector field on $\Gamma(t)$ which depends on the geometric quantities of $\Gamma(t)$. For examples, the velocity of a surface evolving under mean curvature flows is given by

$$v = -Hn = \Delta_{\Gamma(t)}\mathrm{id}, \tag{1.2}$$

where H and n are the mean curvature and the unit outward normal vector on the surface $\Gamma(t)$, respectively. The relation $-Hn = \Delta_{\Gamma(t)}\mathrm{id}$ holds for an arbitrary smooth surface, where id denotes the restriction to $\Gamma(t)$ of identity function on $\mathbb{R}^{d+1}$ defined by $\mathrm{id}(x) \equiv x$. The velocity of a surface evolving under Willmore flow and surface

*Faculty of Computational Mathematics and Cybernetics, Shenzhen MSU-BIT University, Shenzhen 518172, P.R. China. E-mail address: duanbeiping@smbu.edu.cn

†Department of Applied Mathematics, The Hong Kong Polytechnic University, Hong Kong. E-mail address: buyang.li@polyu.edu.hk

diffusion are given by

$$v = \Big(\Delta_\Gamma H - \frac{1}{2}|H|^2 H + |\nabla_\Gamma n|^2 H\Big) n \quad \text{and} \quad v = (\Delta_\Gamma H)\, n, \tag{1.3}$$

respectively. These geometric evolution equations have been intensively studied computationally in the last decades; see [12, 17, 26, 38, 45].

The numerical approximation of surface evolution under geometric flows was first addressed by Dziuk in [19], where he proposed the first parametric finite element method (FEM) for approximating mean curvature flow of closed surfaces in the three-dimensional space. For a given approximate two-dimensional surface $\Gamma_h^j \subset \mathbb{R}^3$ generated by finite elements, Dziuk's parametric FEM computes a parametrization $u_h^{j+1} : \Gamma_h^j \to \mathbb{R}^3$ of the unknown surface $\Gamma_h^{j+1} = u_h^{j+1}(\Gamma_h^j)$ based on the following weak formulation on the known surface Γ_h^j: Find u_h^{j+1} in the three-dimensional vector-valued finite element space $S_h(\Gamma_h^j)^3$ such that

$$\int_{\Gamma_h^j} \frac{u_h^{j+1} - \mathrm{id}}{\tau} \cdot \chi_h + \int_{\Gamma_h^j} \nabla_{\Gamma_h^j} u_h^{j+1} \cdot \nabla_{\Gamma_h^j} \chi_h = 0 \quad \forall\, \chi_h \in S_h(\Gamma_h^j)^3. \tag{1.4}$$

Then the discrete flow map $X_h^{j+1} : \Gamma_h^0 \to \Gamma_h^{j+1}$ can be updated as $X_h^{j+1} = u_h^{j+1} \circ X_h^j$. Since the parametric FEM was proposed by Dziuk in 1990, it was widely used for approximating the evolution of surfaces under various geometric flows, including mean curvature flow, surface diffusion, Willmore flow, Helfrich flow, and so on; see [13, 14, 22]. There are also increasing interests in developing numerical methods for partial differential equations on evolving surfaces; see [15, 18, 23, 24, 34, 36, 40], or refer to [25] for a comprehensive review. The rigorous proof of convergence of parametric FEMs is still challenging for geometric flows of closed surfaces in the three-dimensional space. The convergence of Dziuk's parametric FEMs for curve shortening flow was proved for both semi-discretization in space and full discretization for finite elements of degree $k \geq 1$; see [16, 20, 21, 41, 46]. However, the convergence of Dziuk's parametric FEMs for mean curvature flow of closed surfaces was proved only for semi-discretization in space with finite elements of degree $k \geq 6$; see [2, 35]. This is mainly due to the lack of full H^1 ellipticity of the bilinear form appearing in Dziuk's parametric FEM. Before the work of [2, 35], the convergence of parametric FEMs for mean curvature flow and Willmore flow was proved by Kovács, Li & Lubich in [31, 33] based on reformulations of these geometric flows in terms of the evolution equations of mean curvature and normal vector.

One of the main difficulties in approximating geometric flows of surface by parametric FEMs is that, as time increases, the nodes may cluster and the mesh may become distorted, which often causes breakdown of computation. In this case, Bänsch, Morin & Nochetto proposed certain mesh redistribution technique in [3] to redistribute the mesh points when the nodes cluster and mesh becomes distorted. Another approach to redistributing the mesh points for computational parametric geometric flows is to use harmonic map from a reference surface with good distribution of mesh points; see [43, Chapter 3]. Similar techniques were also used for surface remeshing; see [39, 42].

Differently from the mesh redistribution approach, in their pioneering articles [7–9], Barrett, Garcke & Nürnberg defined a weak formulation for the normal component of the velocity equation and allowed the approximate surface to have a tangential motion implicitly determined by requiring the mapping from Γ_h^j to Γ_h^{j+1} to be a

discrete harmonic map. This class of methods (which we refer to as the BGN methods) has been successful in improving the mesh quality and the performance of numerical approximations without using mesh redistribution techniques. For example, the BGN method for mean curvature flow can be written as: Find $u_h^{j+1} \in S_h(\Gamma_h^j)^3$ and $H_h^{j+1} \in S_h(\Gamma_h^j)$ satisfying the following weak formulation:

$$\begin{aligned} \Big(\frac{u_h^{j+1} - \mathrm{id}}{\tau} \cdot \hat{n}_h^j, \xi_h\Big)_{\Gamma_h^j}^h + \Big(H_h^{j+1}, \xi_h\Big)_{\Gamma_h^j}^h &= 0 \quad \forall \xi_h \in S(\Gamma_h^j) \\ \Big(H_h^{j+1}\hat{n}_h^j, \chi_h\Big)_{\Gamma_h^j}^h - \int_{\Gamma_h^j} \nabla_{\Gamma_h^j} u_h^{j+1} \cdot \nabla_{\Gamma_h^j} \chi_h &= 0 \quad \forall \chi_h \in S(\Gamma_h^j)^3 \end{aligned} \tag{1.5}$$

where the bracket with superscript h denotes the mass-lumping inner product on the surface Γ_h^j, and $\hat{n}_h^j$ is an averaged unit normal vector at the nodes of Γ_h^j. In this algorithm, only the normal velocity of the surface is specified explicitly by the first relation of (1.5), while an artificial tangential velocity is implicitly determined by the second relation of (1.5). The tangential velocity is intended to distribute the mesh points more equally and correspondingly improve the mesh quality of the numerically computed surfaces. In [7, Remark 2.4] and a recently published review article [12, §4.6], Barrett, Garcke & Nürnberg show that if the spatially semidiscrete or nonlinearly implicit BGN methods for the evolution of one-dimensional curves have solutions, then the adjacent edges have equal length if they are not parallel. This partly explains why the tangential velocity given by the BGN methods could distribute the mesh points more equally for the evolution of the one-dimensional curves. The rigorous proof of the convergence of BGN methods for geometric flows still remains open for both curves and surfaces. In practice, the BGN methods have been successful in improving the mesh quality for a wide class of geometric flows which may cause breakdown of computation in the parametric FEMs when there is no artificial tangential velocity.

The BGN methods have also been extended by many others in developing numerical methods for different applications, such as the simulation of interface evolution in two-phase Navier–Stokes flow [10, 11, 27, 28] and solid-state dewetting with contact line migration [5, 48]. Recently, Bao et al. have developed energy-stable and volume-preserving parametric FEMs with artificial tangential velocity in the spirit of the BGN methods in [6, 47] and [4] for surface diffusion with contact line migration and axisymmetric geometric evolution equations, respectively.

In addition to the BGN methods, Elliott & Fritz introduced the DeTurck flow in [37], which reparametrizes the original geometric flow by the harmonic map heat flow from a reference space. The new system obtained after reparametrization contains some tangential velocity which could improve the mesh points distribution on the approximate surface. In particular, the discretization of the new system leads to better mesh quality in some benchmark examples. Another advantage of this approach is that it allows one to prove, at least for the curve shortening flow, the convergence of evolving surface FEM.

In a more recent article [30], Hu & Li show that, as the time stepsize tends to zero, the velocity produced by the BGN method formally tends to a limit velocity w satisfying

$$\begin{aligned} w \cdot n &= v \cdot n \\ \Delta_\Gamma w &= \kappa n, \end{aligned} \tag{1.6}$$

where v is the velocity in the original geometric flow and κ is some auxiliary function. It is shown that the tangential velocity determined by equation (1.6) actually minimizes the instantaneous rate of deformation of the surface. This formal derivation explains, in some sense, why the tangential velocity produced by the BGN method tends to maintain good mesh quality on the approximate surface in the continuous limiting situation. In [30] it is shown that the tangential velocity determined by (1.6) could be coupled with the reformulation of mean curvature flow and Willmore flow by Kovács, Li & Lubich in [31, 33], which allow people to establish stability and convergence of parametric FEMs for these fundamental geometric flows by using the matrix-vector formulation of parametric FEMs in [32] for finite elements of degree $k \geq 2$. The advantage of this approach is that it allows one to approximate the geometric quantities with high-order accuracy and with rigorous analysis for the stability and convergence of numerical approximations. In long-time simulations, however, the evolution equations of n and H used in this approach often produce accumulation errors which make the numerical solutions of n and H differ from the geometric quantities of the approximate surface. This history effect needs to be eliminated by resetting n and H to be the geometric quantities of the approximate surface once the errors reach a tolerance.

In this article, we propose a new class of methods which combines some advantages of the following three classes of methods for improving the mesh quality of numerical approximations: the BGN methods developed in [7–9, 12], the DeTurck techniques introduced in [37], and the artificial tangential velocity defined in [30]. Extensive numerical experiments are provided to demonstrate the effectiveness of the proposed method for several benchmark examples which typically require artificial tangential motions to improve the mesh quality. The numerical results in this article lead to the following observations:

1. In the new class of methods, the shapes of the triangles on the numerically computed surface Γ_h^n are as good as the shapes of the triangles on the initial surface Γ_h^0. This leads to better mesh quality and numerical results than other available methods in some benchmark examples which typically require artificial tangential motions to prevent mesh distortion and breakdown of computation; see Figures 3.3, 3.6, and 3.8.

2. In the new class of methods, the mesh points of Γ_h^n may have non-uniform distribution with locally refined graded mesh towards the locations which correspond to the corners and edges of Γ_h^0; see Figure 3.8. Since the shapes of the triangles are good and the maximal mesh size remains small, the automatic generation of such graded mesh leads to *adaptive mesh* which improves the accuracy of the numerical approximations in the presence of corner and edge singularities; see Example 3.6 and Table 3.5.

3. For the new class of methods proposed in this article, high-order time discretizations are stable with improved accuracy and mesh quality. This is different from the BGN methods which only allow first-order time discretization by the Euler method. High-order time discretizations by the backward difference formula, based on the BGN methods, become unstable probably because that the continuous formulation of the BGN method does not have a unique solution (an arbitrary tangential motion is allowed to exist).

4. The proposed methods do not explicitly have the geometric structure-preserving properties, for example, surface area decrease in mean curvature flow and

enclosed volume conservation in surface diffusion. Nevertheless, in all the numerical examples, the proposed methods yield correct solutions with improved mesh quality. The development of algorithms which have as good mesh quality as the proposed methods in this article, while preserving the geometric structures such as surface area decrease in mean curvature flow and enclosed volume conservation in surface diffusion, is interesting and non-trivial.

2. The numerical methods. In this section, we first formulate the abstract geometric PDEs with an artificial tangential velocity in the continuous setting, and then present the weak formulations, time discretizations and fully discrete parametric FEMs for mean curvature flow, surface diffusion and Willmore flow.

2.1. Formulation of geometric PDEs with artificial tangential velocity. The new class of methods proposed in this article are simultaneously inspired by the following three classes of methods for improving the mesh quality of numerical approximations: the BGN methods developed in [7–9, 12], the DeTurck techniques introduced in [37], and the artificial tangential velocity defined in [30].

Firstly, the tangential velocities given by the BGN methods are determined by requiring the map from Γ_h^j to Γ_h^{j+1} to be a harmonic map, and the artificial tangential velocity in [30] is equivalent to requiring the velocity to be harmonic; correspondingly, the tangential velocity produced by the BGN method, as well as the method in [30], minimizes the deformation between the triangles of Γ_h^{j+1} and Γ_h^j.

Secondly, the DeTurck technique is equivalent to requiring the map from a reference surface to Γ_h^{j+1} to satisfy the harmonic map heat flow; correspondingly, the tangential velocity produced by the DeTurck technique drives the mesh points of Γ_h^{j+1}, in the limiting situation as $t \to \infty$, to a discrete harmonic map.

Motivated by these methods, we propose a tangential velocity which requires the map from a reference surface $\mathcal{M}$ to $\Gamma(t)$ to be harmonic. On the one hand, this corresponds to changing Γ_h^j to a fixed reference surface $\mathcal{M}$; on the other hand, this corresponds to considering the limiting situation $t \to \infty$ in the DeTurck technique (so the harmonic map heat flow reduces to a harmonic map). Correspondingly, the numerically computed surface is approximately conformal to the reference surface $\mathcal{M}$ on which the triangulation has good mesh quality.

However, differently from the formulation of the DeTurck technique used in [37], we formulate the equations in light of (1.6) by utilizing an auxiliary Lagrange multiplier κ which makes the geometric PDEs formally well-posed under the constraint of harmonic mapping. Specifically, we define an artificial tangential velocity by requiring that the map $X(\cdot,t) : \mathcal{M} \to \mathbb{R}^{d+1}$ which determines the surface $\Gamma(t) = \{X(p,t) : p \in \mathcal{M}\}$, $t \in [0,T]$, satisfies the following relations:

$$\begin{cases} \dfrac{\partial X}{\partial t} \cdot (n \circ X) = (v \cdot n) \circ X, \\ \qquad -\Delta_{\mathcal{M}} X = (\kappa n) \circ X. \end{cases} \tag{2.1}$$

where v is the velocity of the surface which depends on the geometric quantities of $\Gamma(t)$, and κ is a scalar-valued Lagrange multiplier, which arises when requiring the map from $\mathcal{M}$ to $\Gamma(t)$ to be a harmonic map, or equivalently, when minimizing the Dirichlet energy

$$E[X(\cdot,t)] = \frac{1}{2} \int_{\mathcal{M}} |\nabla_{\mathcal{M}} X(\cdot,t)|^2 \tag{2.2}$$

under the constraint

$$\frac{\partial X}{\partial t} \cdot (n \circ X) = (v \cdot n) \circ X.$$

Theoretically, for the map $X(\cdot, t) : \mathcal{M} \to \Gamma[X(\cdot, t)]$ to be harmonic, the expression

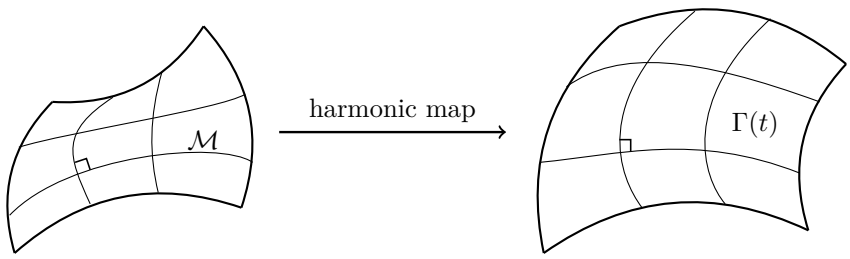

Fig. 2.1. *Harmonic map from the tangent space of $\mathcal{M}$ to the tangent space of $\Gamma(t)$. In our scheme, the normal velocity is determined by $v \cdot n$ and the tangent motion is determined by requiring the map is harmonic. A harmonic map is conformal between genus zero closed surfaces and therefore preserves the intersection angle between two lines (thus keeping the shape of the triangles almost unchanged). For more general surfaces, a harmonic map is also very close to a conformal map; see [29, pp. 296-297].*

of the Lagrange multiplier is given by $\kappa = \mathrm{tr}[\nabla_{\mathcal{M}} X (\nabla_{\Gamma(t)} n)^\top (\nabla_{\mathcal{M}} X)^\top])$, see [44, pp. 191-193] or [43, Chapter 2, (2.10)]. However, in the numerical computation, the two unknowns X and κ should be solved by the parametric FEM using the two relations in (2.1).

The system of equations in (2.1) is a unified abstract formulation of our method in the continuous setting, where the velocity v should be replaced by the geometric quantities in a specific geometric flow, such as mean curvature flow, surface diffusion and Willmore flow. This is described in the next subsection through the weak formulations and the time discretizations.

2.2. Weak formulations and time discretizations. For simplicity, we denote $X(t) = X(\cdot, t)$ and consider the following weak formulation for (2.1): Find an immersion $X(t) : \mathcal{M} \to \mathbb{R}^{d+1}$ which determines the surface $\Gamma(t) = \{X(p, t) : p \in \mathcal{M}\}$ and a function $\kappa : \Gamma(t) \to \mathbb{R}$ satisfying the following equations:

$$\begin{aligned} \int_{\Gamma(t)} \Big(\frac{\partial X}{\partial t} \circ X^{-1}\Big) \cdot \xi n &= \int_{\Gamma(t)} v \cdot \xi n \qquad && \forall\, \xi \in H^1(\Gamma(t)) \\ \int_{\mathcal{M}} \nabla_{\mathcal{M}} X \cdot \nabla_{\mathcal{M}} \eta &= \int_{\mathcal{M}} [(\kappa n) \circ X] \cdot \eta && \forall\, \eta \in H^1(\mathcal{M})^{d+1}. \end{aligned} \tag{2.3}$$

In the computation it is often more convenient to formulate (2.3) on the evolving surface $\Gamma(t)$, i.e.,

$$\begin{cases} \displaystyle\int_{\Gamma(t)} \Big(\frac{\partial X}{\partial t} \circ X^{-1}\Big) \cdot \xi n = \int_{\Gamma(t)} v \cdot \xi n & \forall\, \xi \in H^1(\Gamma(t)) \\ \displaystyle\int_{\Gamma(t)} \nabla_{\Gamma(t)} \mathrm{id}\, J^{-1} \cdot (\nabla_{\Gamma(t)} \eta) \sqrt{\det(J)} = \int_{\Gamma(t)} \kappa n \cdot \eta \sqrt{\det(J)} & \forall\, \eta \in H^1(\Gamma(t))^{d+1}, \end{cases} \tag{2.4}$$

where $\sqrt{\det(J)}$ denotes the ratio between the surface area elements on $\mathcal{M}$ and $\Gamma(t)$, with the Jacobian matrix $J = \nabla_{\Gamma(t)} X^{-1} (\nabla_{\Gamma(t)} X^{-1})^\top + nn^\top$.

By this approach, using the identity $\Delta_{\Gamma(t)}\mathrm{id} = -Hn$, the weak formulation for mean curvature flow, surface diffusion and Willmore flow are given by

- Mean curvature flow:

$$\begin{aligned} \int_{\Gamma(t)} \Big(\frac{\partial X}{\partial t} \circ X^{-1}\Big) \cdot \xi n + \int_{\Gamma(t)} \nabla_{\Gamma(t)}\mathrm{id} \cdot \nabla_{\Gamma(t)}(\xi n) = 0 \\ \int_{\Gamma(t)} \nabla_{\Gamma(t)}\mathrm{id} J^{-1} \cdot (\nabla_{\Gamma(t)}\eta)\sqrt{\det(J)} - \int_{\Gamma(t)} \kappa n \cdot \eta \sqrt{\det(J)} = 0. \end{aligned} \tag{2.5}$$

- Surface diffusion:

$$\begin{aligned} \int_{\Gamma(t)} \Big(\frac{\partial X}{\partial t} \circ X^{-1}\Big) \cdot \xi n + \int_{\Gamma(t)} \nabla_{\Gamma(t)} H \cdot \nabla_{\Gamma(t)}\xi = 0 \\ \int_{\Gamma(t)} \nabla_{\Gamma(t)}\mathrm{id} \cdot \nabla_{\Gamma(t)}(\phi n) - \int_{\Gamma(t)} H\phi = 0 \\ \int_{\Gamma(t)} \nabla_{\Gamma(t)}\mathrm{id}\, J^{-1} \cdot (\nabla_{\Gamma(t)}\eta)\sqrt{\det(J)} - \int_{\Gamma(t)} \kappa n \cdot \eta \sqrt{\det(J)} = 0. \end{aligned} \tag{2.6}$$

- Willmore flow:

$$\begin{aligned} \int_{\Gamma(t)} \Big(\frac{\partial X}{\partial t} \circ X^{-1}\Big) \cdot \xi n + \int_{\Gamma(t)} \nabla_{\Gamma(t)} H \cdot \nabla_{\Gamma(t)}\xi - \int_{\Gamma(t)} GH\xi = 0 \\ \int_{\Gamma(t)} \nabla_{\Gamma(t)}\mathrm{id} \cdot \nabla_{\Gamma(t)}(\phi n) - \int_{\Gamma(t)} H\phi = 0 \\ \int_{\Gamma(t)} \nabla_{\Gamma(t)}\mathrm{id}\, J^{-1} \cdot (\nabla_{\Gamma(t)}\eta)\sqrt{\det(J)} - \int_{\Gamma(t)} \kappa n \cdot \eta \sqrt{\det(J)} = 0, \end{aligned} \tag{2.7}$$

  with $G = -\frac{1}{2}|H|^2 + |\nabla_{\Gamma(t)} n|^2$.

In the formulations above, $\xi \in H^1(\Gamma(t))$, $\phi \in H^1(\Gamma(t))$ and $\eta \in H^1(\Gamma(t))^{d+1}$.

These weak formulations can be discretized in time by the semi-implicit Euler methods given below, based on a partition $0 = t_0 < t_1 < t_2 < \cdots < t_{N-1} < t_N = T$ of the time interval $[0, T]$ with stepsize $\tau_j = t_{j+1} - t_j$.

- Mean curvature flow: For a given surface Γ^j which approximates the surface $\Gamma(t_j)$, find a parametrization $u^{j+1} : \Gamma^j \to \mathbb{R}^{d+1}$ of the approximate surface $\Gamma^{j+1} = u^{j+1}(\Gamma^j)$ and a scalar function $\kappa^{j+1} \in L^2(\Gamma^j)$ such that

$$\begin{aligned} \int_{\Gamma^j} \frac{u^{j+1} - \mathrm{id}}{\tau_j} \cdot \xi n^j + \int_{\Gamma^j} \nabla_{\Gamma^j} u^{j+1} \cdot \nabla_{\Gamma^j}(\xi n^j) = 0 \\ \int_{\Gamma^j} \nabla_{\Gamma^j} u^{j+1}\, (J^j)^{-1} \cdot (\nabla_{\Gamma^j}\eta)\sqrt{\det(J^j)} - \int_{\Gamma^j} \kappa^{j+1} n^j \cdot \eta \sqrt{\det(J^j)} = 0 \end{aligned} \tag{2.8}$$

  for $\xi \in H^1(\Gamma^j)$ and $\eta \in H^1(\Gamma^j)^{d+1}$, where J^j denotes the Jacobian matrix corresponding to Γ^j. The flow map $X^{j+1} : \mathcal{M} \to \Gamma^{j+1}$ can be updated as $X^{j+1} = u^{j+1} \circ X^j$.

- Surface diffusion: Find $u^{j+1} \in H^1(\Gamma^j)^{d+1}$ and $H^{j+1}, \kappa^{j+1} \in L^2(\Gamma^j)$ such that

$$\begin{aligned} \int_{\Gamma^j} \frac{u^{j+1} - \mathrm{id}}{\tau_j} \cdot \xi n^j + \int_{\Gamma^j} \nabla_{\Gamma^j} H^{j+1} \cdot \nabla_{\Gamma^j}\xi = 0 \\ \int_{\Gamma^j} \nabla_{\Gamma^j} u^{j+1} \cdot \nabla_{\Gamma^j}(\phi n^j) - \int_{\Gamma^j} H^{j+1}\phi = 0 \\ \int_{\Gamma^j} \nabla_{\Gamma^j} u^{j+1}\, (J^j)^{-1} \cdot (\nabla_{\Gamma^j}\eta)\sqrt{\det(J^j)} - \int_{\Gamma^j} \kappa^{j+1} n^j \cdot \eta \sqrt{\det(J^j)} = 0 \end{aligned} \tag{2.9}$$

for $\xi \in H^1(\Gamma^j)$, $\phi \in H^1(\Gamma^j)$ and $\eta \in H^1(\Gamma^j)^{d+1}$. The flow map $X^{j+1} : \mathcal{M} \to \Gamma^{j+1}$ can be updated as $X^{j+1} = u^{j+1} \circ X^j$.

The time discretization of Willmore flow based on the weak formulation in (2.7) and the semi-implicit Euler method could be written down similarly as that for surface diffusion.

Higher-order time discretizations could also be used for the weak formulations in (2.5)–(2.7). We present the semi-implicit Euler method and the two-step backward differentiation formula (BDF2) in a unified form in the fully discrete parametric FEMs by utilizing the nodal vector which determines the approximate surface.

2.3. The fully discrete parametric FEMs. Let $\Gamma_h^j = \bigcup_{K \in \mathscr{K}^j} K$ be the polyhedral surface which approximates $\Gamma(t_j)$ in the method, where $\mathscr{K}^j$ denotes the set of simplices on the surface Γ_h^j. The finite element space on Γ_h^j is defined as

$$S_h(\Gamma_h^j) = \big\{ w \in C(\Gamma_h^j) : w|_K \text{ is linear for } \forall K \in \mathscr{K}^j \big\}.$$

Let $\mathbf{u}^{j+1}$ be the vector of nodal values of the finite element function $u_h^{j+1} \in S_h(\Gamma_h^j)$. The surface Γ_h^{j+1} is uniquely determined by the nodal vector $\mathbf{u}^{j+1}$. We denote by $\delta_t u_h^{j+1}$ the finite element function in $S_h(\Gamma_h^j)$ with nodal vector $\delta_t \mathbf{u}^{j+1}$, where

$$\delta_t \mathbf{u}^{j+1} := \frac{\mathbf{u}^{j+1} - \mathbf{u}^j}{\tau_j} \qquad \text{for the Euler method,}$$

$$\delta_t \mathbf{u}^{j+1} := \frac{\tau_{j-1} + 2\tau_j}{\tau_j(\tau_{j-1} + \tau_j)} \mathbf{u}^{j+1} - \frac{\tau_{j-1} + \tau_j}{\tau_{j-1}\tau_j} \mathbf{u}^j + \frac{\tau_j}{\tau_{j-1}(\tau_{j-1} + \tau_j)} \mathbf{u}^{j-1} \qquad \text{for BDF2.}$$

In the semi-implicit Euler method, we define $\hat{\Gamma}_h^{j+1} = \Gamma_h^j$. In the semi-implicit BDF2 method, we denote by $\hat{\Gamma}_h^{j+1}$ the extrapolated surface determined by Γ_h^j and Γ_h^{j-1}. That is, $\hat{\Gamma}_h^{j+1}$ is a polyhedral surface collocating at the nodes in the nodal vector $\hat{\mathbf{u}}^{j+1} = \frac{\tau_{j-1}+\tau_j}{\tau_{j-1}}(\mathbf{u}^j - \mathbf{u}^{j-1}) + \mathbf{u}^{j-1}$.

Let $\hat{n}_K^{j+1}$ be the unit normal vector on the simplex $K \subset \hat{\Gamma}_h^{j+1}$ and define the averaged normal vector $\hat{n}_h^{j+1} \in S_h(\hat{\Gamma}_h^{j+1})^{d+1}$ to be the finite element function with the following value at a node $p \in \hat{\Gamma}_h^{j+1}$:

$$\hat{n}_h^{j+1}(p) = \frac{\sum_{K \ni p} |K| \hat{n}_K^{j+1}}{\left| \sum_{K \ni p} |K| \hat{n}_K^{j+1} \right|}, \tag{2.10}$$

where the summation extends over all simplices K which contains p as a vertex.

The fully discrete parametric FEM for mean curvature flow reads: Find $u_h^{j+1} \in S_h(\hat{\Gamma}_h^{j+1})^{d+1}$ and $\kappa_h^{j+1} \in S_h(\hat{\Gamma}_h^{j+1})$ such that

$$\begin{cases} \displaystyle\int_{\hat{\Gamma}_h^{j+1}} \delta_t u_h^{j+1} \cdot \xi_h \hat{n}_h^{j+1} + \int_{\hat{\Gamma}_h^{j+1}} \nabla_{\hat{\Gamma}_h^{j+1}} u_h^{j+1} \cdot \nabla_{\hat{\Gamma}_h^{j+1}} (\xi_h \hat{n}_h^{j+1}) = 0 \\ \displaystyle\int_{\hat{\Gamma}_h^{j+1}} \nabla_{\hat{\Gamma}_h^{j+1}} u_h^{j+1} (\hat{J}_h^{j+1})^{-1} \cdot \nabla_{\hat{\Gamma}_h^{j+1}} \eta_h \sqrt{\det(\hat{J}_h^{j+1})} - \int_{\hat{\Gamma}_h^{j+1}} \kappa_h^{j+1} \hat{n}_h^{j+1} \cdot \eta_h \sqrt{\det(\hat{J}_h^{j+1})} = 0 \end{cases} \tag{2.11}$$

for $\xi_h \in S_h(\hat{\Gamma}_h^{j+1})$ and $\eta_h \in S_h(\hat{\Gamma}_h^{j+1})^{d+1}$, where $\hat{J}_h^{j+1}$ is the Jacobian matrix between an approximate reference surface $\mathcal{M}_h$ and the extrapolated surface $\hat{\Gamma}_h^{j+1}$, given by

$$\hat{J}_h^{j+1}|_K = \nabla_{\hat{\Gamma}_h^{j+1}} Y_h (\nabla_{\hat{\Gamma}_h^{j+1}} Y_h)^\top + \hat{n}_K^{j+1} (\hat{n}_K^{j+1})^\top, \quad \forall K \in \hat{\Gamma}_h^{j+1}, \tag{2.12}$$

with $Y_h \in S_h(\hat{\Gamma}_h^{j+1})^{d+1}$ being the finite element function with nodal values corresponding to the nodes of $\mathcal{M}_h$. Thus $\det(\hat{J}_h^{j+1})$ is a piecewise constant which can be evaluated easily in the practical computation.

Similarly, the fully discrete parametric FEM for surface diffusion reads: Find $u_h^{j+1} \in S_h(\hat{\Gamma}_h^{j+1})^{d+1}$ and $H_h^{j+1}, \kappa_h^{j+1} \in S_h(\hat{\Gamma}_h^{j+1})$ such that

$$\begin{cases} \displaystyle\int_{\hat{\Gamma}_h^{j+1}} \delta_t u_h^{j+1} \cdot \xi_h \hat{n}_h^{j+1} + \int_{\hat{\Gamma}_h^{j+1}} \nabla_{\hat{\Gamma}_h^{j+1}} H_h^{j+1} \cdot \nabla_{\hat{\Gamma}_h^{j+1}} \xi_h = 0 \\ \displaystyle\int_{\hat{\Gamma}_h^{j+1}} \nabla_{\hat{\Gamma}_h^{j+1}} u_h^{j+1} \cdot \nabla_{\hat{\Gamma}_h^{j+1}} (\phi_h \hat{n}_h^{j+1}) - \int_{\hat{\Gamma}_h^{j+1}} H_h^{j+1} \cdot \phi_h = 0 \\ \displaystyle\int_{\hat{\Gamma}_h^{j+1}} \nabla_{\hat{\Gamma}_h^{j+1}} u_h^{j+1} (\hat{J}_h^{j+1})^{-1} \cdot \nabla_{\hat{\Gamma}_h^{j+1}} \eta_h \sqrt{\det(\hat{J}_h^{j+1})} - \int_{\hat{\Gamma}_h^{j+1}} \kappa_h^{j+1} \hat{n}_h^{j+1} \cdot \eta_h \sqrt{\det(\hat{J}_h^{j+1})} = 0 \end{cases} \tag{2.13}$$

for $\xi_h \in S_h(\hat{\Gamma}_h^{j+1})$, $\phi_h \in S_h(\hat{\Gamma}_h^{j+1})$ and $\eta_h \in S_h(\hat{\Gamma}_h^{j+1})^{d+1}$.

Since the normal vector we used in this article is the averaged normal vector $\hat{n}_h^{j+1} \in S_h(\hat{\Gamma}_h^{j+1})^{d+1}$ which is globally continuous and piecewise linear, the gradient of $\hat{n}_h^{j+1}$ is well defined as a piecewise constant function, which is used in the second equation of (2.13) in the term $\nabla_{\hat{\Gamma}_h^{j+1}}(\phi_h \hat{n}_h^{j+1})$. Therefore, the full discretization of Willmore flow could be written down similarly as that for surface diffusion.

In the fully discrete parametric FEMs, the reference surface $\mathcal{M}_h$ cannot be chosen arbitrarily. Otherwise, the harmonic map constraint will lead to large tangent motion which pollutes the accuracy of the numerical approximation. In this article, we always choose $\mathcal{M}_h$ to be the initial approximate surface Γ_h^0, which is assumed to have good mesh quality.

2.4. Two-stage algorithms. The linearly implicit algorithms given in (2.11) and (2.13) are convenient for computation and lead to good mesh quality, as shown in the numerical experiments in the next section. However, these is no explicit mathematical proof which guarantees that these algorithms preserve the energy diminishing property of the continuous models (the energy associated to the surface decreases due to the gradient flow structure of these geometric flows). Instead of calculating the parametrization u_h^{j+1} directly, as shown in (2.11) and (2.13), one could also consider a two-stage algorithm which first computes an intermediate-step approximate surface based on the BGN methods and then improve the mesh quality with a tangential motion based on the methodology developed in this article.

For example, for mean curvature flow, we could first find an intermediate-step approximate surface by Dziuk's method or the BGN method, i.e., compute $\tilde{u}_h^{j+1} \in S_h(\Gamma_h^j)^{d+1}$ such that

$$\int_{\Gamma_h^j} I_h[\delta_t \tilde{u}_h^{j+1} \cdot \xi_h] + \int_{\Gamma_h^j} \nabla_{\Gamma_h^j} \tilde{u}_h^{j+1} \cdot \nabla_{\Gamma_h^j} \xi_h = 0 \quad \forall\, \xi_h \in S_h(\Gamma_h^j)^{d+1}, \tag{2.14}$$

where I_h denotes the Lagrangian interpolation operator onto the finite element space on the surface. This yields an approximate surface $\widetilde{\Gamma}_h^{j+1} = \tilde{u}_h^{j+1}(\Gamma_h^j)$ with area decreasing, i.e., $|\widetilde{\Gamma}_h^{j+1}| \le |\Gamma_h^j|$, according to the energy decreasing property of Dziuk's method.

Next, we let the mesh points of $\widetilde{\Gamma}_h^{j+1}$ move tangentially to improve the mesh quality, by finding a tangential motion $w_h^{j+1} \in S_h(\widetilde{\Gamma}_h^{j+1})$ such that $w_h^{j+1} \cdot \widetilde{n}_h^{j+1} = 0$ at

the nodes of $\widetilde{\Gamma}_h^{j+1}$ and an auxiliary function $\kappa_h^{j+1} \in S_h(\widetilde{\Gamma}_h^{j+1})$ satisfying the following weak formulation:

$$\begin{aligned}\int_{\widetilde{\Gamma}_h^{j+1}} \nabla_{\widetilde{\Gamma}_h^{j+1}}(\mathrm{id} + w_h^{j+1})(\tilde{J}_h^{j+1})^{-1} \cdot \nabla_{\widetilde{\Gamma}_h^{j+1}} \eta_h \sqrt{\det(\tilde{J}_h^{j+1})} \\ - \int_{\widetilde{\Gamma}_h^{j+1}} \kappa_h^{j+1} \widetilde{n}_h^{j+1} \cdot \eta_h \sqrt{\det(\tilde{J}_h^{j+1})} = 0\end{aligned} \tag{2.15}$$

for $\eta_h \in S_h(\widetilde{\Gamma}_h^{j+1})^{d+1}$, where $\widetilde{n}_h^{j+1}$ denotes the averaged normal vector on $\widetilde{\Gamma}_h^{j+1}$, and $\tilde{J}_h^{j+1}$ is the Jacobian between $\mathcal{M}_h$ and $\widetilde{\Gamma}_h^{j+1}$, which is defined similar to (2.12).

Then the map $\mathrm{id} + w_h^{j+1} : \widetilde{\Gamma}_h^{j+1} \to \Gamma_h^{j+1}$ defines the approximate surface Γ_h^{j+1} at time level t_{j+1}. This type of algorithms decreases the area in the first stage. While the area cannot be shown decreasing in the second stage, the tangential motion in the second step is expected to improve the mesh quality rather than to evolve the surface according to mean curvature flow. This is the intuition which motivates us to introduce the two-stage method as a compromise when the construction of strictly area-descreasing methods is still challenging.

Similarly, for surface diffusion and Willmore flow, one could also first find an intermediate-step approximate surface based on the BGN methods and then find a tangential motion based on the weak formulation in (2.15). The numerical experiments in the next section show that these two-stage algorithms have excellent performance in all the benchmark examples.

The development of algorithms which have similar mesh quality as the proposed methods, while directly reducing the energy associated with the surface without differing by the additional tangential motion, is interesting and non-trivial.

Remark 2.1. In [43, Chapter 4], the author proposed to remesh a given polyhedral surface by using a harmonic map from a reference approximate surface $\mathcal{M}_h$ (which interpolates a reference smooth surface $\mathcal{M}$ with a well-distributed mesh points) to a new approximate surface Γ_h^{j+1} with enhanced mesh quality. The proposed method involved the following steps: (1) Compute a discrete harmonic map $W_h : \widetilde{\Gamma}_h^{j+1} \to \widetilde{\mathcal{M}}_h$ from an approximate surface $\widetilde{\Gamma}_h^{j+1}$ to an unknown approximate surface $\widetilde{\mathcal{M}}_h$ that interpolates the reference smooth surface $\mathcal{M}$. (2) Lift the vertices of the reference approximate surface $\mathcal{M}_h$ onto $\widetilde{\mathcal{M}}_h$. (3) Find the image of the lifted vertices under the inverse map $W_h^{-1} : \widetilde{\mathcal{M}}_h \to \widetilde{\Gamma}_h^{j+1}$. These images of the lifted vertices constitute the new approximate surface Γ_h^{j+1}. In contrast to this approach, our one-stage method aims to compute an improved approximate surface directly, rather than generating a suboptimal surface and subsequently remeshing it. Our two-stage method can be viewed as a splitting of the one-stage method into two stages, with the second stage focusing on calculating a tangential velocity that renders the map from $\mathcal{M}_h$ to Γ_h^{j+1} discretely harmonic. This eliminates the need for finding a discrete harmonic map in the reverse direction, i.e., from $\widetilde{\Gamma}_h^{j+1}$ to an unknown approximate $\widetilde{\mathcal{M}}_h$ that interpolates the reference smooth surface $\mathcal{M}$, and avoids computing the lift of vertices from one approximate surface to another approximate surface. Consequently, our techniques bear a stronger resemblance to the BGN methods than the remeshing method discussed in [43, Chapter 4].

3. Numerical experiments. In this section we present numerical experiments on several examples, in comparison with the BGN methods and DeTurck flow method, to demonstrate the effectiveness of the proposed methods in improving both the mesh

quality and the accuracy of numerical approximations to the surface evolution under mean curvature flow and surface diffusion. We refer to the proposed methods in Sections 2.3 and 2.4 as the one-stage method and two-stage method, respectively. All the computations are implemented in `Python` with the FEM package Firedrake; see `https://firedrakeproject.org/citing.html`

Throughout, we denote by N_p and N_T the number of vertices and triangles in the mesh, respectively. We denote by $U(t_n)$ the numerical solution at time level $t = t_n$, with the jth component $U_j(t_n) \in \mathbb{R}^{d+1}$ representing the position of the jth vertex at time $t = t_n$. The mesh quality for a two-dimensional surface is measured by

$$\sigma_{\max} = \max_{T \in \mathcal{T}_h} \frac{h(T)}{r(T)}, \tag{3.1}$$

as in [37, eq. (7.3)], where $h(T)$ and $r(T)$ denote the diameter of the circumcircle and the diameter of the maximal inscribed circle of a triangle T, respectively. Furthermore, we denote by E_h the surface area of the numerically computed surface in the following examples.

3.1. Mean curvature flow.

Example 3.1. We test the convergence of the proposed method for mean curvature flow with the initial surface being the unit sphere. In this case, the exact solution at time $t < 0.25$ is known to be the sphere with radius $r(t) = \sqrt{1 - 4t}$.

To test the convergence in time, we triangulate the initial surface using a sufficiently small mesh size, with $N_T = 81920$ triangles and $N_p = 40962$ vertices, so that the error from the spatial discretization is negligibly small in observing the convergence in time.

The errors of the numerical solutions with several different time stepsizes and the corresponding convergence rates are presented in Table 3.1. The error of the numerical solution at time t_n given by the proposed method with stepsize τ and number of vertices N_p is measured by

$$\text{Error}(t_n, \tau, N_p) = \max_{j=1,2,\cdots,N_p} \big| |U_j(t_n)| - r(t_n) \big|. \tag{3.2}$$

The convergence rate in time is calculated by the following formula for two consecutive stepsizes τ_1 and τ_2:

$$\text{Convergence rate} := \frac{\ln(\text{Error}(0.2, \tau_1, N_p)/\text{Error}(0.2, \tau_2, N_p))}{\ln(\tau_1/\tau_2)}. \tag{3.3}$$

From Table 3.1 we can see that the time discretizations by the Euler method and the BDF2 method have first- and second-order convergence, respectively.

To test the convergence in space, we use BDF2 method with a sufficiently small time stepsize $\tau = 2 \times 10^{-4}$ so that the error from the time discretization is negligibly small in observing the convergence in space. The errors of the numerical solutions defined by (3.2) at $t_n = 0.2$ are computed with several different spatial meshes, with the following numbers of vertices and triangles:

$$(N_p, N_T) = (624, 1280), (2562, 5120), (10242, 20480), (40962, 81920).$$

We present the errors of the numerical solutions at $t = 0.2$ and the corresponding convergence rates in Table 3.2, where the convergence rates are calculated by

$$\text{Convergence rate} := \frac{\ln(\text{Error}(0.2, \tau, N_p)/\text{Error}(0.2, \tau, N_p'))}{\ln(N_p'/N_p)}, \tag{3.4}$$

with N_p and N_p' denoting the numbers of the vertices in two consecutive meshes. The numerical results show that the errors of the proposed method are $\mathcal{O}(N_p^{-1})$, i.e., optimal with respect to the number of degrees of freedom (this corresponds to second-order convergence with respect to the mesh size).

TABLE 3.1
Example 3.1: Error *at* $t = 0.2$ *with different time stepsizes.*

τ	1×10^{-2}	5×10^{-3}	2.5×10^{-3}	1.25×10^{-3}
Semi-implicit Euler	4.388×10^{-2}	2.405×10^{-2}	1.265×10^{-2}	6.468×10^{-2}
Convergence rate	–	0.90	0.93	0.97
Semi-implicit BDF2	3.424×10^{-3}	8.340×10^{-4}	1.535×10^{-4}	3.881×10^{-5}
Convergence rate	–	2.00	2.44	1.98

TABLE 3.2
Example 3.1: Error *at* $t = 0.2$ *with different spatial meshes.*

N_p	642	2562	10242	40962
Error	5.834e-03	1.490e-03	3.801e-04	8.287e-05
Convergence rate	–	0.99	0.99	1.10

Example 3.2. We consider a benchmark example for testing the effectiveness in approximating mean curvature flow; see [30,37]. The initial surface is a dumbbell-shape surface given by the following local parametrization

$$x = \begin{bmatrix} \cos\varphi \\ (0.6\cos^2\varphi + 0.4)\cos\theta\sin\varphi \\ (0.6\cos^2\varphi + 0.4)\sin\theta\sin\varphi \end{bmatrix}, \qquad \theta \in [0, 2\pi), \quad \varphi \in [0, \pi]. \tag{3.5}$$

The dumbbell-shape surface will evolve to a sphere in the end. However, the numerical approximation of this surface evolution process requires the algorithm to contain certain artificial tangential velocity to improve the mesh quality and prevent mesh distortion. Otherwise, the computation will break down when the mesh becomes distorted. This happens in Dziuk's method and many other methods which do not contain proper artificial tangential velocity to improve the mesh quality.

In the numerical simulation, we triangulate the initial surface into 5024 triangles with 2510 vertices; see Figure 3.1(a). The numerical results given by the BGN method and two methods proposed in this article are presented in Figure 3.1. In order to resolve the solution close to the final blow-up time, we change the time stepsize from $\tau = 1 \times 10^{-4}$ to $\tau = 2 \times 10^{-7}$ when $t \geq 0.0908$ for the BGN scheme and our one-stage method. For the two-stage method we change $\tau = 1 \times 10^{-4}$ to $\tau = 1 \times 10^{-7}$ when $t \geq 0.09$ since finer mesh is needed in this scheme. The numerical results show that the proposed methods are successful in producing the correct solution for this benchmark example as the BGN method. Note that if we use a smaller stepsize $\tau = 1 \times 10^{-7}$ in the BGN scheme for $t \geq 0.09$, then it produces worse mesh; see Figure 3.2 (a). The methods proposed in this article do not encounter this issue; see Figure 3.2 (b) for the one-stage method and Figure 3.1 (g) for the two-stage method for the numerical results with $\tau = 1 \times 10^{-7}$.

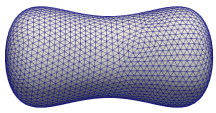

(a) Initial surface, $E_h = 6.276$

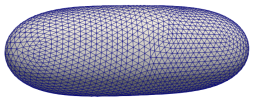

(b) BGN at $t = 0.0751$, $E_h = 1.040$

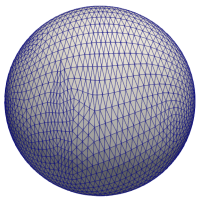

(c) BGN at $t = 0.0908262$, $E_h = 5.629 \times 10^{-10}$

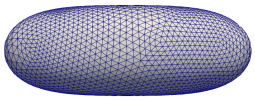

(d) Our one-stage method at $t = 0.0751$, $E_h = 1.033$

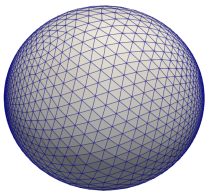

(e) Our one-stage method at $t = 0.0908026$, $E_h = 1.236 \times 10^{-11}$

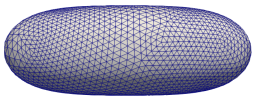

(f) Our two-stage method at $t = 0.0751$, $E_h = 1.048$

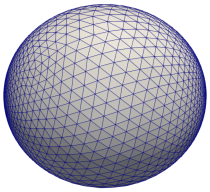

(g) Our two-stage method at $t = 0.0907248$, $E_h = 7.127 \times 10^{-8}$

Fig. 3.1. *Example 3.2: Numerical results given by the BGN method and our methods (images are rescaled).*

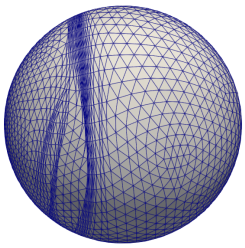

(a) BGN at $t = 0.0906355$, $E_h = 1.242 \times 10^{-10}$

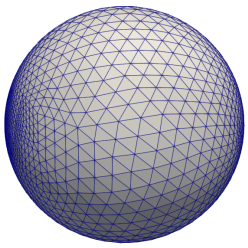

(b) Our one-stage method at $t = 0.0905324$, $E_h = 4.675 \times 10^{-10}$

Fig. 3.2. *Example 3.2: Numerical results given by the BGN method and our method with* $\tau = 1 \times 10^{-7}$ *for* $t \geq 0.09$ *(images are rescaled).*

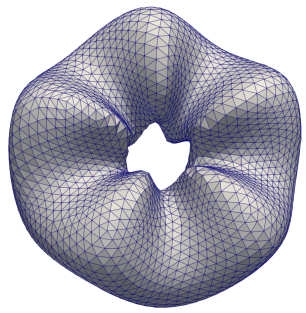

(a) Initial surface, $E_h = 30.3937$

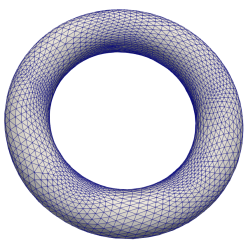

(b) Our one-stage scheme: $t = 0.235$, $E_h = 3.4788$

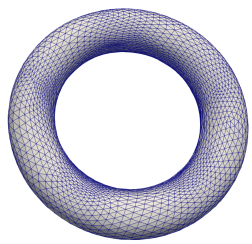

(c) Our two-stage scheme: $t = 0.235$, $E_h = 3.4963$

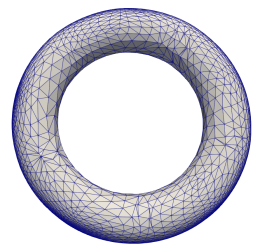

(d) Dziuk's scheme: $t = 0.235$, $E_h = 3.4975$

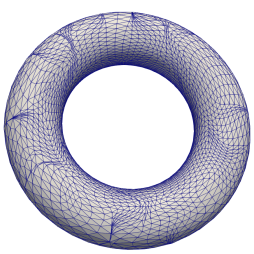

(e) BGN scheme: $t = 0.235$, $E_h = 4.1279$

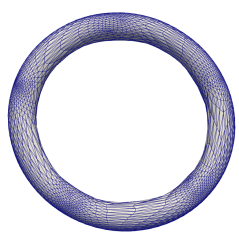

(f) DeTurck flow method: $t = 0.235, \alpha = 1$, $E_h = 2.2246$

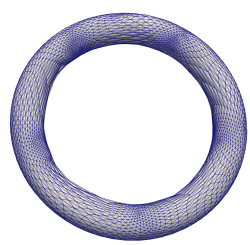

(g) DeTurck flow method: $t = 0.235, \alpha = 10^{-4}$, $E_h = 2.6671$

Fig. 3.3. *Example 3.3: Numerical results given by our methods, the Dziuk's method, the BGN method, and the DeTurck flow technique (images are rescaled).*

Example 3.3. We consider another example for mean curvature flow, with the initial surface given by the following parametrization:

$$x = \begin{bmatrix} (1 + 0.65\cos\varphi)\cos\theta \\ (1 + 0.65\cos\varphi)\sin\theta \\ 0.65\sin\varphi + 0.3\sin(5\theta) \end{bmatrix}, \quad \theta \in [0, 2\pi), \quad \varphi \in [0, 2\pi). \tag{3.6}$$

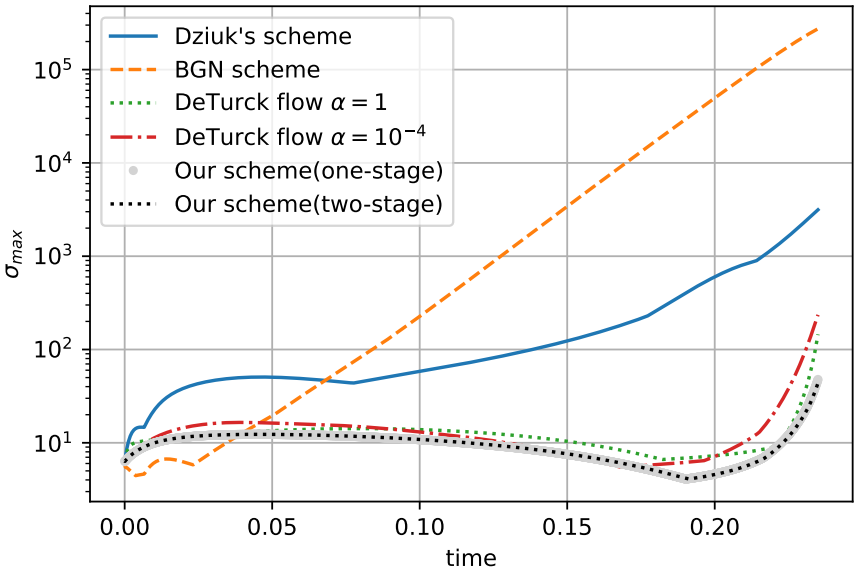

Fig. 3.4. *Example 3.3: Evolution of mesh quality in different methods.*

The initial surface has large curvature at some places and evolves with large deformation. In the raised places on the surface, the points move towards the inside of the torus, while points in the concave areas move outward. The surface velocity field exhibit rapid changes with respect to position. Consequently, an effective tangential motion strategy is needed to prevent mesh distortion and breakdown of computation.

The numerical results given by several different methods, including Dziuk's method, the BGN method, the DeTurck flow by Elliott & Fritz [37, Algorithm 5.3] and the method proposed in this article (with the semi-implicit Euler scheme), are presented in Figure 3.3 with common mesh (6208 triangles with 3104 vertices) time stepsize $\tau = 1 \times 10^{-4}$. One can see that the mesh produced by the BGN scheme degenerates in some places. The evolution of mesh quality in different methods is presented in Figure 3.4. The parameter $\alpha > 0$ in the method of DeTurck flow represents the inverse diffusion constant of the harmonic map heat flow. Roughly speaking, smaller α induces larger tangential motion in the scheme. It is interesting to see that the mesh size of the triangles produced by Dziuk's method is larger than the mesh size in the BGN method, while the shape of triangles produced by Dziuk's method in this example is better than the shape of triangles produced by the BGN method when t exceeds some t_0, as shown in Figure 3.4. From these Figures we see that the proposed method keeps the mesh quality good in this challenging example. The BGN method and the DeTurck flow method could yield good shapes of the surface by using a smaller mesh size in space. If the parameter 0.65 in (3.6) is replaced by 0.7 then the inner surface shrinks to a point singularity; see [37, Fig. 26(f)]; if the parameter 0.65 is replaced by 0.6, then it shrinks to a torus-type singularity; see [37, Fig. 26(d)].

3.2. Surface diffusion.

Example 3.4. We test the convergence of the proposed method for surface diffusion with the initial surface $\Gamma(0)$ being a $1:1:2$ ellipsoid with unit semi-minor axis. The surface will evolve to a steady-state sphere with radius $r = 2^{1/3} \approx 1.25992$. We compare our numerical solutions with this sphere to test the convergence in approximating the steady state.

To test the convergence rate in space, we adopt BDF2 scheme in time with a sufficiently small stepsize $\tau = 1 \times 10^{-3}$ so that the error from time discretization is negligibly small in observing the convergence in space. The errors of the numerical solutions given by several different meshes at $T = 5$ (when the numerical solutions already reach the steady state) are presented in Table 3.3, which shows that the spatial discretization errors of the proposed method are proportional to N_p^{-1}.

To test the convergence rate in time, we triangulate the initial surface almost uniformly with a sufficiently small mesh size, with 2562 vertices and 5120 triangles, and compute the numerical solution at $T = 1$ with several different time stepsizes. The reference solution U^{ref} is computed by using the BDF2 scheme with a sufficiently small stepsize $\tau = 1 \times 10^{-4}$. The errors between the numerical solutions and the reference solution, defined by

$$\text{Error}(t_n; \tau, N_p) := \max_{j=1,2,\cdots,N_p} \left| U_j^{\text{ref}} - U_j \right| \tag{3.7}$$

are presented in Table 3.4 at $t_n = 1$ with several different stepsizes. The numerical results in Table 3.4 show that the errors of the numerical solutions given by the semi-implicit Euler scheme and BDF2 scheme are $\mathcal{O}(\tau)$ and $\mathcal{O}(\tau^2)$, respectively.

Table 3.3
Example 3.4: Space discretization errors at $t = 5$.

N_p	162	642	2562	10242
Error	2.295e-2	7.621e-3	2.085e-3	5.903e-4
Convergence rate	–	0.90	0.94	0.91

Table 3.4
Example 3.4: Time discretization errors at $t = 1$.

τ	2×10^{-2}	1×10^{-2}	5×10^{-3}	2.5×10^{-3}	1.25×10^{-3}
BDF2	4.512e-3	1.103e-3	2.238e-4	4.670e-5	9.717e-6
Convergence rate	–	2.03	2.30	2.26	2.27
Euler	4.736e-3	2.685e-3	1.510e-3	8.220e-4	4.351e-4
Convergence rate	–	0.82	0.83	0.88	0.92

Example 3.5. We consider the merging process of two spheres of radius $r = 1$ under surface diffusion. The initial surface is triangulated with 6432 vertices and 12860 triangles, as shown in Figure 3.5, where the maximal mesh size is about 0.15 and refined to 0.01 around the contact line between the two balls. The distance between the centers of the two spheres is 1.96.

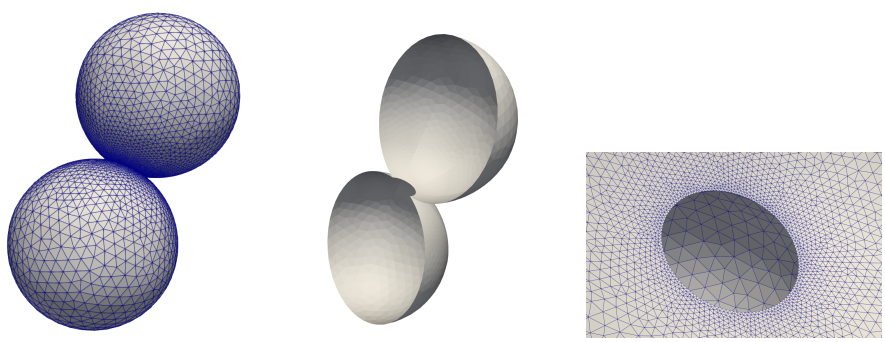

(a) Initial surface (b) Cross section of the initial surface (c) Close-up of the contact area (view from inside)

Fig. 3.5. *Triangulation of the initial surface in Example 3.5, the contact line is a circle with radius* $\sqrt{1-0.98^2}$.

We present the numerical simulations given by the proposed methods and the BGN method with common mesh and stepsize $\tau = 2\times 10^{-4}$ in Figure 3.6, and present the evolution of the mesh quality defined in (3.1) in Figure 3.7. The numerical results in Figures 3.6 and 3.7 show that the proposed methods keep the mesh quality good in this challenging example.

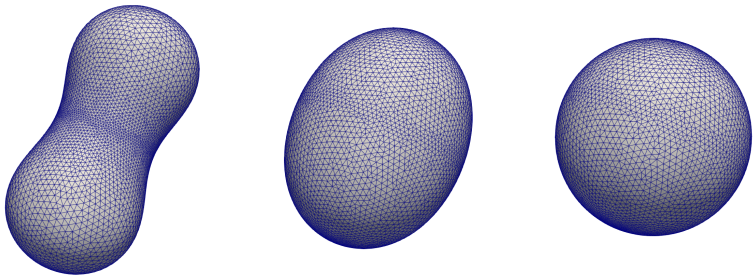

(a) Our one-stage scheme: $t = 0.02$ (b) Our one-stage scheme: $t = 0.3$ (c) Our one-stage scheme: $t = 0.7$

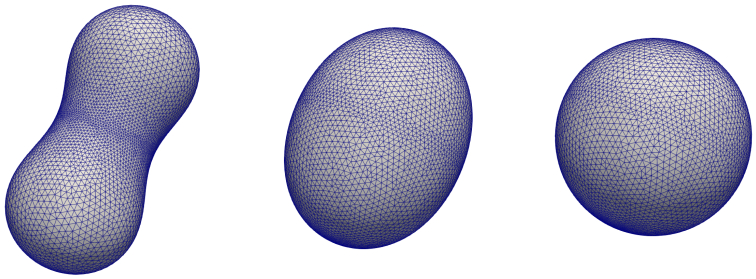

(d) Our two-stage scheme: $t = 0.02$ (e) Our two-stage scheme: $t = 0.3$ (f) Our two-stage scheme: $t = 0.7$

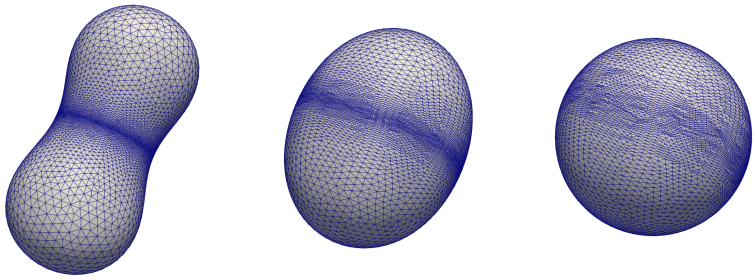

(g) BGN method: $t = 0.02$ (h) BGN method: $t = 0.3$ (i) BGN method: $t = 0.7$

Fig. 3.6. *Example 3.5: Merging of the two spheres in Figure 3.5 under surface diffusion (images are rescaled).*

Example 3.6. We consider the evolution of a $1 : 1 : 6$ box under surface diffusion. The initial surface is triangulated into 3264 triangles with 1634 vertices, as shown in Figure 3.8 (a). The numerical simulations by the BGN method and the proposed one-stage Euler method with common mesh and stepsize $\tau = 1 \times 10^{-4}$ are presented in Figure 3.8, which shows that the BGN method leads to mesh degeneration and

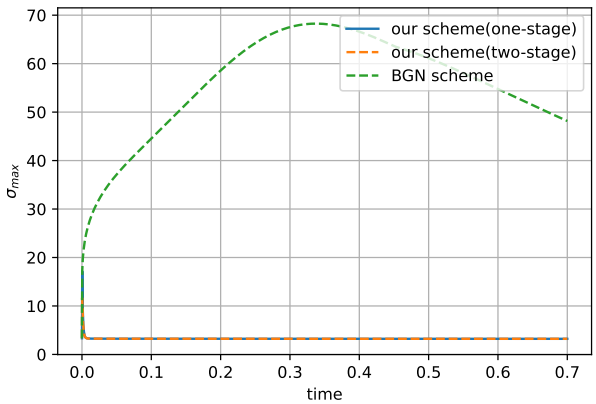

Fig. 3.7. *Example 3.5: Evolution of mesh quality in different methods.*

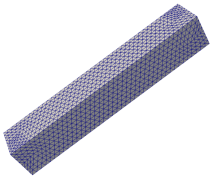

(a) Initial surface

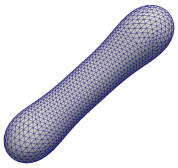

(b) BGN: $t = 0.05$

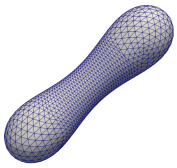

(c) BGN: $t = 0.1$

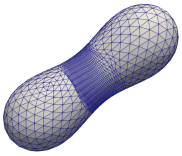

(d) BGN: $t = 0.25$

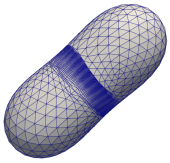

(e) BGN: $t = 0.35$

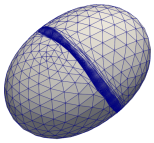

(f) BGN: $t = 0.5$

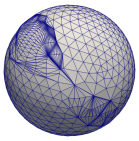

(g) BGN: $t = 2.7$

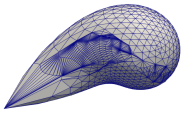

(h) BGN: $t = 2.7845$

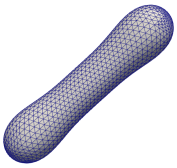

(i) Our method: $t = 0.05$

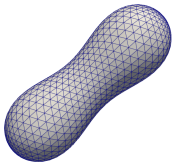

(j) Our method: $t = 0.25$

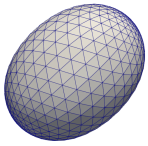

(k) Our method: $t = 0.5$

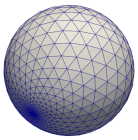

(l) Our method: $t = 5$

Fig. 3.8. *Example 3.6: Evolution of a long box under surface diffusion (images are rescaled).*

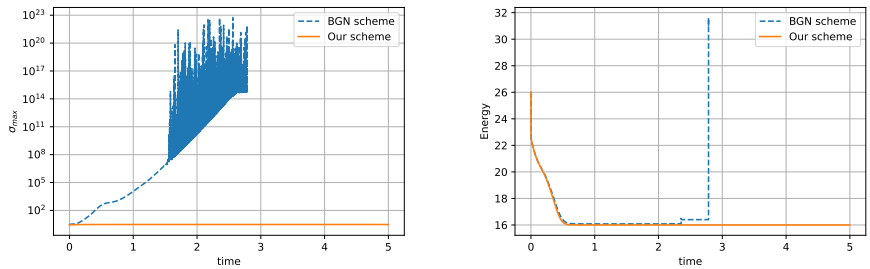

(a) Evolution of mesh quality (b) Evolution of energy

Fig. 3.9. *Example 3.6: Evolution of mesh quality and energy in different methods.*

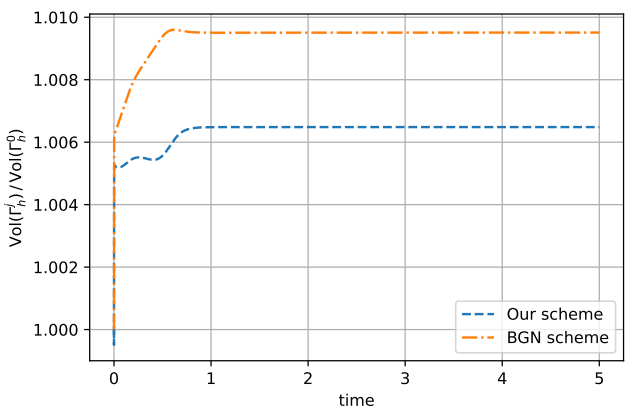

Fig. 3.10. *Example 3.6: Enclosed volume with respect to time.*

eventually breakdown of the computation at $t = 2.7845$, while the proposed method keeps the mesh quality good throughout. The evolution of mesh quality and energy for both methods are presented in Figure 3.9, which shows that the proposed method keeps the mesh quality good and the energy decreasing. Note that the mesh produced by the BGN method in this example does not degenerate when a larger stepsize is used.

The convergence rate to the steady state with respect to the number of vertices N_p is presented in Table 3.5 by the same method as Example 3.4. Despite the initial surface is nonsmooth with corners and edges, the proposed method converges to the steady state with optimal order in space probably due to the following property of method: The mesh points in the proposed method automatically refine towards the locations which correspond to the corners and edges in the initial surface. This leads to *adaptive mesh* which improves the accuracy of the numerical solutions in the presence of corner and edge singularities.

It is known that surface diffusion preserves the enclosed volume, which can be used to test the accuracy of the numerical approximations to the evolving surface under surface diffusion. Regarding this aspect, we present the numerical results of

$\mathrm{Vol}(\Gamma_h^j)/\mathrm{Vol}(\Gamma_h^0)$ produced by the BGN method and the proposed one-stage method in Figure 3.10, with $\mathrm{Vol}(\Gamma_h)$ representing the volume enclosed by the polyhedral surface Γ_h. Since the surface area decreases rapidly at the beginning, we use the graded mesh $t_j = 5\left(\frac{j}{5000}\right)^2$ for $j = 1, 2, \cdots, 5000$ (rather than uniformly small stepsizes) to save the computational cost. With these time stepsizes, the mesh produced by the BGN scheme does not degenerate up to $t \leq 5$. From Figure 3.10 we see that the proposed method is of similar accuracy as the BGN method in approximating the enclosed volume of the evolving surface.

Table 3.5
Example 3.6: Convergence to the steady state with several different meshes.

N_p	104	410	1634	6530
Error	1.383e-01	3.268e-02	6.553e-03	1.202e-03
Convergence rate	–	1.05	1.16	1.22

4. Conclusions. We have proposed a new class of methods which combines some advantages of the BGN methods, the DeTurck techniques, and the artificial tangential velocity defined in [30] for improving the mesh quality in approximating surface evolution under geometric flows. The proposed methods contain an artificial tangential velocity and a Lagrange multiplier which requires the map from a reference surface to the unknown surface to be harmonic at the continuous level. The ideas could also be used to construct two-stage algorithms, with the first stage using available parametric FEMs such as Dziuk's method or the BGN method which preserves certain geometric structures, and the second stage using the methodology proposed in this article only for improving the mesh quality by a tangential motion. We have presented extensive numerical experiments and simulations to demonstrate the effectiveness of the proposed method for several examples which typically require artificial tangential motions to prevent mesh distortion and breakdown of computation. The convergence of the proposed methods is tested for a shrinking sphere under mean curvature flow and the evolution of an ellipsoid and a box under surface diffusion. In the numerical simulation of mean curvature flow and surface diffusion, the proposed one-stage and two-stage methods have both shown their capability to improve the mesh quality over available methods. The theoretical proof of convergence of the proposed class of methods for the various geometric flows is still challenging. The stability and convergence of finite element approximations to surface evolution, with artificial tangential velocity to improve the mesh quality, can be proved by using the evolution equations of mean curvature and normal vector; see [30] and [1] for geometric flows and surface evolution under a prescribed velocity field, respectively.

In the example of surface diffusion with corner and edge singularities on the initial surface, the proposed method automatically generates adaptive mesh (from a quasi-uniform mesh) which improves the accuracy of the numerical approximations. This is an attractive property of the proposed method in addition to its capability for improving the mesh quality.

The proposed method does not explicitly have the geometric structure-preserving properties, for example, surface area decrease in mean curvature flow and enclosed volume conservation in surface diffusion. The development of algorithms which have

as good mesh quality as the proposed methods in this article, while preserving the geometric structures such as surface area decrease in mean curvature flow and enclosed volume conservation in surface diffusion, is interesting and non-trivial.

Acknowledgement. This work is supported in part by National Natural Science Foundation of China (grant No. 12201418), a grant from the Research Grants Council of the Hong Kong Special Administrative Region, China (GRF Project No. PolyU15303022), and an internal grant of The Hong Kong Polytechnic University (Project ID: P0038843, Work Programme: ZVX7).

REFERENCES

[1] G. Bai, J. Hu, and B. Li, *A convergent evolving finite element method with artificial tangential motion for surface evolution under a prescribed velocity field*, (submitted).

[2] G. Bai and B. Li, *Erratum: Convergence of Dziuk's semidiscrete finite element method for mean curvature flow of closed surfaces with high-order finite elements*, SIAM J. Numer. Anal., accepted (2023).

[3] E. Bänsch, P. Morin, and R. Nochetto, *A finite element method for surface diffusion: The parametric case*, J. Comput. Phys., 203 (2005), pp. 321–343.

[4] W. Bao, H. Garcke, R. Nürnberg, and Q. Zhao, *Volume-preserving parametric finite element methods for axisymmetric geometric evolution equations*, J. Comput. Phys., 460 (2022), p. 111180.

[5] W. Bao, W. Jiang, Y. Wang, and Q. Zhao, *A parametric finite element method for solid-state dewetting problems with anisotropic surface energies*, J. Comput. Phys., 330 (2017), pp. 380–400.

[6] W. Bao and Q. Zhao, *A structure-preserving parametric finite element method for surface diffusion*, SIAM J. Numer. Anal., 59 (2021), pp. 2775–2799.

[7] J. Barrett, H. Garcke, and R. Nürnberg, *A parametric finite element method for fourth order geometric evolution equations*, J. Comput. Phys., 222 (2007), pp. 441–467.

[8] J. Barrett, H. Garcke, and R. Nürnberg, *On the parametric finite element approximation of evolving hypersurfaces in* $\mathbb{R}^3$, J. Comput. Phys., 227 (2008), pp. 4281–4307.

[9] J. Barrett, H. Garcke, and R. Nürnberg, *Parametric approximation of Willmore flow and related geometric evolution equations*, SIAM J. Sci. Comput., 31 (2008), pp. 225–253.

[10] J. Barrett, H. Garcke, and R. Nürnberg, *Eliminating spurious velocities with a stable approximation of viscous incompressible two-phase Stokes flow*, Comput. Methods Appl. Mech. Engrg., 267 (2013), pp. 511–530.

[11] J. Barrett, H. Garcke, and R. Nürnberg, *A stable parametric finite element discretization of two-phase Navier–Stokes flow*, J. Sci. Comput., 63 (2015), pp. 78–117.

[12] J. Barrett, H. Garcke, and R. Nürnberg, *Parametric finite element approximations of curvature-driven interface evolutions*, in Handbook of Numerical Analysis, vol. 21, Elsevier, 2020, pp. 275–423.

[13] A. Bonito, R. H. Nochetto, and M. S. Pauletti, *Parametric FEM for geometric biomembranes*, J. Comput. Phys., 229 (2010), pp. 3171–3188.

[14] E. Bänsch, P. Morin, and R. H. Nochetto, *A finite element method for surface diffusion: the parametric case*, J. Comput. Phys., 203 (2005), pp. 321–343.

[15] K. C. Cheung, L. Ling, and S. J. Ruuth, *A localized meshless method for diffusion on folded surfaces*, J. Comput. Phys., 297 (2015), pp. 194–206.

[16] K. Deckelnick and G. Dziuk, *On the approximation of the curve shortening flow*, in Calculus of variations, applications and computations (Pont-à-Mousson, 1994), vol. 326 of Pitman Res. Notes Math. Ser., Longman Sci. Tech., Harlow, 1995, pp. 100–108.

[17] K. Deckelnick, G. Dziuk, and C. Elliott, *Computation of geometric partial differential equations and mean curvature flow*, Acta Numer., 14 (2005), pp. 139–232.

[18] K. Deckelnick and V. Styles, *Stability and error analysis for a diffuse interface approach to an advection–diffusion equation on a moving surface*, Numer. Math., 139 (2018), pp. 709–741.

[19] G. Dziuk, *An algorithm for evolutionary surfaces*, Numer. Math., 58 (1990), pp. 603–611.

[20] G. Dziuk, *Convergence of a semi-discrete scheme for the curve shortening flow*, Math. Models Methods Appl. Sci., 4 (1994), pp. 589–606.

[21] G. Dziuk, *Discrete anisotropic curve shortening flow*, SIAM J. Numer. Anal., 36 (1999), pp. 1808–1830.

[22] G. Dziuk, *Computational parametric Willmore flow*, Numer. Math., 111 (2008), pp. 55–80.
[23] G. Dziuk and C. M. Elliott, *Finite elements on evolving surfaces*, IMA J. Numer. Anal., 27 (2007), pp. 262–292.
[24] G. Dziuk and C. M. Elliott, *A fully discrete evolving surface finite element method*, SIAM J. Numer. Anal., 50 (2012), pp. 2677–2694.
[25] G. Dziuk and C. M. Elliott, *Finite element methods for surface pdes*, Acta Numerica, 22 (2013), pp. 289–396.
[26] K. Ecker, *Regularity theory for mean curvature flow*, Springer, 2012.
[27] G. Fu, *Arbitrary Lagrangian–Eulerian hybridizable discontinuous Galerkin methods for incompressible flow with moving boundaries and interfaces*, Comput. Methods Appl. Mech. Eng., 367 (2020), p. 113158.
[28] S. Ganesan, A. Hahn, K. Simon, and L. Tobiska, *ALE-FEM for two-phase and free surface flows with surfactants*, in Transport Processes at Fluidic Interfaces, Advances in Mathematical Fluid Mechanics, Springer International Publishing, 2017, pp. 5–31.
[29] X. Gu and S.-T. Yau, *Computational Conformal Geometry*, International Press and Higher Education Press, 2020.
[30] J. Hu and B. Li, *Evolving finite element methods with an artificial tangential velocity for mean curvature flow and willmore flow*, Numer. Math., 152 (2022), pp. 127–181.
[31] B. Kovács, B. Li, and C. Lubich, *A convergent evolving finite element algorithm for Willmore flow of closed surfaces*, Numer. Math., (2021), pp. 595–643.
[32] B. Kovács, B. Li, C. Lubich, and C. Power Guerra, *Convergence of finite elements on an evolving surface driven by diffusion on the surface*, Numer. Math., 137 (2017), pp. 643–689.
[33] B. Kovács, B. Li, and C. Lubich, *A convergent evolving finite element algorithm for mean curvature flow of closed surfaces*, Numer. Math., 143 (2019), pp. 797–853.
[34] C. Lehrenfeld, M. A. Olshanskii, and X. Xu, *A stabilized trace finite element method for partial differential equations on evolving surfaces*, SIAM J. Numer. Anal., 56 (2018), pp. 1643–1672.
[35] B. Li, *Convergence of Dziuk's semidiscrete finite element method for mean curvature flow of closed surfaces with high-order finite elements*, SIAM J. Numer. Anal., 59 (2021), pp. 1592–1617.
[36] Y. Li, X. Qi, and J. Kim, *Direct discretization method for the Cahn–Hilliard equation on an evolving surface*, J. Sci. Comput., 77 (2018), pp. 1147–1163.
[37] C M Elliott and H. Fritz, *On approximations of the curve shortening flow and of the mean curvature flow based on the Deturck trick*, IMA J. Numer. Anal., 37 (2017), pp. 543–603.
[38] C. Mantegazza, *Lecture Notes on Mean Curvature Flow*, Progress in Mathematics, Volume 290. Birkhäuser, Corrected Printing 2012.
[39] E. Marchandise, C. C. de Wiart, W. Vos, C. Geuzaine, and J.-F. Remacle, *High-quality surface remeshing using harmonic maps—part ii: Surfaces with high genus and of large aspect ratio*, International Journal for Numerical Methods in Engineering, 86 (2011), pp. 1303–1321.
[40] A. Petras, L. Ling, C. Piret, and S. J. Ruuth, *A least-squares implicit RBF-FD closest point method and applications to PDEs on moving surfaces*, J. Comput. Phys., 381 (2019), pp. 146–161.
[41] P. Pozzi, *Anisotropic curve shortening flow in higher codimension*, Math. Meth. Appl. Sci., 30 (2007), pp. 1243–1281.
[42] J.-F. Remacle, C. Geuzaine, G. Compere, and E. Marchandise, *High-quality surface remeshing using harmonic maps*, International Journal for Numerical Methods in Engineering, 83 (2010), pp. 403–425.
[43] J. Steinhilber, *Numerical analysis for harmonic maps between hypersurfaces and grid improvement for computational parametric geometric flows*, PhD thesis, Dissertation, Albert-Ludwigs-Universität Freiburg, 2014, 2014.
[44] M. Struwe, *Variational methods*, vol. 991, Springer, 2000.
[45] B. White, *Evolution of curves and surfaces by mean curvature*, in Proceedings of the International Congress of Mathematicians, Vol. I (Beijing, 2002), Higher Ed. Press, Beijing, 2002, pp. 525–538.
[46] C. Ye and J. Cui, *Convergence of Dziuk's fully discrete linearly implicit scheme for curve shortening flow*, SIAM J. Numer. Anal., 59 (2021), pp. 2823–2842.
[47] Q. Zhao, W. Jiang, and W. Bao, *An energy-stable parametric finite element method for simulating solid-state dewetting*, IMA J. Numer. Anal., 41 (2020), pp. 2026–2055.
[48] Q. Zhao, W. Jiang, and W. Bao, *A parametric finite element method for solid-state dewetting problems in three dimensions*, SIAM J. Sci. Comput., 42 (2020), pp. B327–B352.